Temperature- and species-dependent quenching of CO *B* probed by two-photon laser-induced fluorescence using a picosecond laser

T. B. Settersten
Combustion Research Facility, Sandia National Laboratories, Livermore, California 94551

A. Dreizler
Fachgebiet Energie- und Kraftwerkstechnik, Technische Universität Darmstadt, 64287 Darmstadt, Germany

R. L. Farrow
Combustion Research Facility, Sandia National Laboratories, Livermore, California 94551

(Received 4 March 2002; accepted 22 May 2002)

We report measurements of the temperature- and species-dependent cross sections for the quenching of fluorescence from the $B\,^1\Sigma^+(v=0)$ state of CO. Cross sections were measured for gas temperatures ranging from 293 K to 1031 K for quenching by H_2, N_2, O_2, CO, H_2O, CO_2, CH_4, He, Ne, Ar, Kr, and Xe. The CO $B\,^1\Sigma^+(v=0)$ state was populated via two-photon excitation ($B\,^1\Sigma^+ \leftarrow\leftarrow X\,^1\Sigma^+$), and the $B\,^1\Sigma^+ \rightarrow A\,^1\Pi$ fluorescence was collected. Quenching cross sections were determined from the dependence of the fluorescence-decay rate on quencher-gas pressure. The temperature dependence of the cross sections is well described by a power law for all but the two weakest quenchers, He and Ne. © *2002 American Institute of Physics.* [DOI: 10.1063/1.1493198]

I. INTRODUCTION

CO is an important component of reacting flows, such as plasmas and flames, and its detection is significant in numerous research fields including planetary atmospheric physics, biochemistry, surface science, and combustion. Laser-induced fluorescence (LIF) detection of CO by two-photon excitation of the Hopfield–Birge electronic transition ($B\,^1\Sigma^+ \leftarrow\leftarrow X\,^1\Sigma^+$) and collection of the blue-to-green emission in the Angström bands ($B\,^1\Sigma^+ \rightarrow A\,^1\Pi$) was first demonstrated by Loge *et al.*[1,2] This technique has received considerable attention for applications in combustion.[3–17] The use of two-photon LIF for determining CO concentrations quantitatively requires a detailed knowledge of the rate of collisional quenching of the $B\,^1\Sigma^+$ state, which can be calculated only if the cross sections for quenching by all collision partners are known.

A direct and accurate way to obtain quenching cross sections is to time-resolve the fluorescence signal following short-pulse laser excitation and to observe the variation of the fluorescence lifetime as a function of the quencher pressure. CO $B\,^1\Sigma^+$ has a natural lifetime of about 22 ns, and collisions with even modest pressures (<10 Torr) of strongly quenching species (e.g., water vapor) reduce the effective fluorescence lifetime to a few nanoseconds.[18] Thus, excitation by standard dye lasers (~10 ns pulses) is insufficient for time-resolved studies. This problem has been circumvented in some cases[1,2,19,20] by Stern–Volmer methods,[21] which extract the quenching cross sections from the pressure dependence of the time-integrated fluorescence. These methods, however, can be unreliable if the fluorescence decay is nonexponential, if radiative trapping is important,[22] or if pressure broadening is significant.[19] Only Agrup and Aldén have presented a time-resolved study of two-photon LIF from CO $B\,^1\Sigma^+$.[10,11] Although they reported a measurement of the CO self-quenching rate coefficient, the principal objective of their work was to measure the $B\,^1\Sigma^+$-state lifetime in hydrocarbon flames; species-specific quenching cross sections were not obtained.

In this article, we describe the continuation of previous work, in which room-temperature quenching cross sections were measured.[18] In the current work, we extend the measurements to elevated temperatures using a new picosecond excitation source and a high-temperature sample cell. Furthermore, a refined data analysis procedure is used to improve the accuracy of the reported quenching cross sections. Species-specific quenching cross sections for CO $B\,^1\Sigma^+$ ($v=0$) in collisions with other CO molecules, rare gases (He, Ne, Ar, Kr, and Xe), and major combustion species (H_2, N_2, O_2, H_2O, CO_2, and CH_4) are reported.

II. EXPERIMENTAL DETAILS

The experimental setup consisted of a picosecond dye laser, a heated cell and a fluorescence detection/recording apparatus.

The picosecond laser was an amplified, distributed-feedback dye laser (DFDL),[23] which is an improved version of that described in Ref. 24. The DFDL and amplifier were pumped by the second harmonic of a regeneratively amplified Nd:YAG laser (Positive Light, ~100 ps pulse duration, 20 Hz repetition rate), which was seeded by an actively mode-locked laser (Lightwave Electronics series 131, ~100-ps pulse duration, 100-MHz repetition rate, ~300-mW output power). The DFDL was operated slightly above threshold to obtain the best pulse stability without producing multiple pulses. Approximately 70 μJ from the pump laser was used to create a 3-mm gain region in a dye cell (containing a solution 800 mg/l of LDS 698 in methanol), producing approximately 40 nJ at 690 nm.

Following a weak spatial filter, the DFDL output was amplified in two side-pumped dye cells using 3 and 2 mJ of 532-nm pump energy, respectively. The first dye cell contained a solution of 200 mg/l of LDS 698 in methanol, while the second cell contained a solution of 33 mg/l. We obtained approximate gains of 5×10^3 and 5 from the first and second amplifiers, respectively, resulting in an 875-μJ, 70-ps, near-transform-limited pulse.

The amplified 690-nm output from the DFDL was frequency tripled in two BBO crystals to produce approximately 125 μJ at 230-nm with a net tripling efficiency of 15%. The resultant pulsewidth was 55 ps, as measured with a streak camera (Hamamatsu M2547). The transform-limited bandwidth of a 55-ps pulse is 0.3 cm^{-1}, and we estimate the UV bandwidth to be approximately 1 cm^{-1}, based on the measured linewidth of the 690-nm light.

The laser beam was aligned along the axis of a 63-cm long, 9-cm diam quartz tube. The cell was capped with a 10-cm diam excimer-grade fused-silica window at the laser input, and with a Brewster-angle fused-silica window at the exit. The laser focused with a 500-mm lens to an elliptical spot at the center of the cell with major and minor full widths at half maximum (FWHM) that were approximately 60 and 30 μm, respectively.

The fluorescence was collected in a backscattering geometry through the input window. Two 76.2-mm diam, 400-mm focal length, glass achromatic lenses were used to collect and focus the fluorescence onto the input slit of a 1/8-m monochromator (Oriel 77250). The exit slit was opened to 3 mm, and a grating with 600 lines per millimeter (Oriel 77919) was used in second order to produce a bandpass of approximately 25 nm centered at 483 nm. Emission was collected primarily from the $B\,^1\Sigma^+\rightarrow A\,^1\Pi(0,1)$ band with small contributions from the (0,0) and (0,2) bands. A microchannel-plate photomultiplier tube (Hamamatsu R3809U, 150-ps risetime, 360-ps falltime) was attached to the monochromator output. The detector was biased with -2.8 kV for all measurements, and signal levels were kept well within the linear range of the detector. The signals were collected and averaged using a digital storage oscilloscope (Tektronix TDS 680B, 1-GHz bandwidth), and the averaged records were downloaded to a computer for analysis.

The quartz cell was mounted inside a commercial tube furnace (MHI model H17HCT). The CO/quencher gas mixtures were heated to temperatures of up to 1031 K. The cell was fitted with five annular fused-silica disks that transmitted the full solid angle defined by the LIF collection optics while reducing radiative losses and improving temperature uniformity in the central region of the cell. The furnace temperature controller maintained the temperature at the center of the cell to within 3 K of the set point. Axial temperature variations were $<1\%$ in the central 4 cm of the cell and $<2\%$ in the central 10 cm.

The cell was evacuated to $\sim10^{-5}$ Torr using an oil-free pumping system consisting of a turbomolecular pump backed by a scroll pump. The cell pressure was monitored with high-precision capacitance manometers (MKS). The capacitance manometers were zeroed at $<10^{-4}$ Torr and calibrated at atmospheric pressure with a Fortin-type mercurial barometer.

All gases, with the exception of H_2O, were reagent grade or better, and were purified further with gas-chromatograph filters: oxygen getters (Matheson 6406-A) were used to purify inert gases and CO individually, while molecular sieves (Matheson 451) were used for the other species. Water vapor was introduced as a quenching gas by pulling the vapor from a second, independently pumped, vacuum cell containing distilled water.

Fluorescence decay curves were collected for each of the quenching gases at 293 K, 536 K, 784 K, and 1031 K. At each temperature setting, the cell was filled with several Torr of He and allowed to stabilize. Following temperature stabilization, the cell was evacuated to $<10^{-4}$ Torr and then filled with CO to produce adequate LIF signals while avoiding radiation trapping and stimulated emission. Typical CO fill pressures were 6, 18, 35, and 50 mTorr for temperatures of 293, 536, 784, and 1031 K, respectively. Higher CO number density could be used at the elevated temperatures owing to the reduction of radiation trapping with increased absorption linewidth. Following the CO fill, 1–2 Torr of He was added to the cell to act as a buffer gas, and the gas mixture was allowed several minutes to stabilize prior to data acquisition. LIF decays were recorded for a sequence of increasing quenching gas pressures. The quenching-gas pressures were chosen so that the highest pressure produced a 160–200 MHz decay rate. For He and Ne, the weakest quenchers, fill pressures were limited to approximately 600 Torr, and the largest decay rates were approximately 110 MHz at 293 K. At each pressure, two or three decays were collected. The partial pressure of each constituent gas in the mixture was determined from cell pressure measurements that were recorded at 1-s intervals during the gas fills and during the acquisition of LIF decays. These pressure records also permitted the measurement of the leak-up rate, resulting from outgassing and leaks in the vacuum cell. Leak-up rates ranged from <1 mTorr/min at 293 K to ~6 mTorr/min at 1031 K. The leak-up gas was treated as an additional component of the mixture, and its partial pressure was determined for each decay measurement.

The consumption of CO by hot O_2 was observed during the O_2 trials at 1031 K. In this case, the CO LIF signal decreased exponentially in time, with a time constant of approximately 2 min. Therefore, the experimental procedure was modified so that decay rates were measured immediately following the addition of O_2 to the cell, and separate CO fills were used for each partial pressure of O_2. Chemical kinetics modeling using CHEMKIN (Ref. 25) indicated that oxidation of CO to CO_2 was occurring, although the predicted rate was much slower than that observed. We estimate that the ratio $[CO_2]$:$[O_2]$ was $<2\%$ for all of the O_2 quenching measurements. Because the quenching rate coefficient (at 1031 K) of CO_2 is comparable to that of O_2, measurements of the latter were not corrected for the presence of CO_2.

Each fluorescence-decay record is 1000 points and consists of a 1000-shot average (50 s). The oscilloscope sampling rate and trigger point were set so that each record included a pre-excitation baseline and at least 8 *e*-folding times

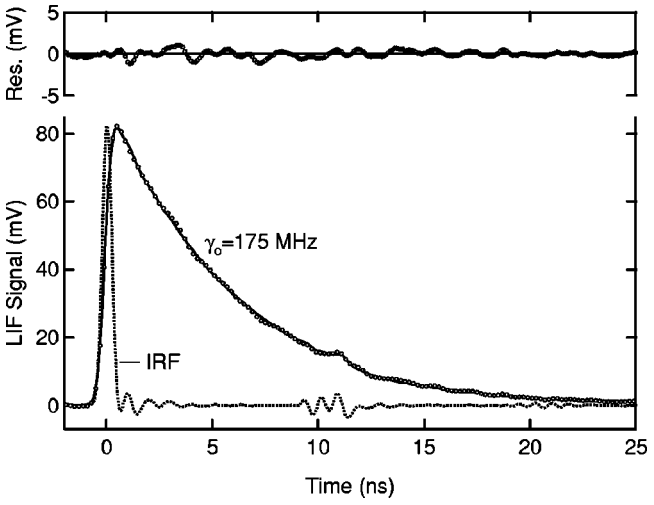

FIG. 1. The IRF for the detection system (dotted curve), and an example of a background-corrected LIF signal (circles, lower panel), the corresponding best-fit model (solid curve), and the fit residual (upper panel) for quenching by H_2O at 784 K. (Every other LIF data point is omitted from the figure for clarity.)

of the LIF decay. Background signals, due to fluorescence from the collection optics induced by scattered laser light, were acquired by detuning the laser from the CO absorption band. At least two background signals per quenching-gas pressure sequence were collected. Background levels were highest at elevated temperatures due to degraded performance of the anti-reflective coating on the laser input window.

We approximate the impulse-response function (IRF) of the detection electronics by detecting Rayleigh scattering from a 55-ps laser pulse. Because the LIF collection optics did not transmit UV wavelengths, the Rayleigh measurement could not be taken with the LIF experimental arrangement. Instead, it was collected in a right-angle scattering geometry using the same filter monochromator. The Rayleigh measurement, shown as the dotted curve in Fig. 1, therefore characterizes the collective response (to a 55-ps pulse) of the detector, the oscilloscope, and the cabling between the detector and the oscilloscope, but not the transit-time spreading introduced by the extended source of fluorescing CO molecules accessed in the backscattering collection geometry of the LIF apparatus. Correction for the latter effect is described subsequently. Note the weak cable reflections evident at 10 and 20 ns in Fig. 1. Although these reflections appear tolerable, they caused least-squares estimates of the fluorescence decay rate, γ_o, to be in error by as much as 10% at the highest decay rates when fitting background-corrected data with a single-exponential function. Furthermore, estimates of γ_o obtained in this way were sensitive to the temporal range of data used in the fit. To eliminate this error, we accounted for the IRF through use of a convolution fitting routine, as described in the next section.

III. ANALYSIS

LIF decays were analyzed using a convolve-and-compare fitting routine to determine γ_o. This routine obtained best-fit parameters for a synthetic decay record by calling STEPIT (Ref. 26) to minimize the sum of squares of the residual differences between the data and the model. The following 6-parameter model produced excellent agreement with the experimental decays:

$$I = I_f(i_o, \gamma_o, t_o) * f * g(\Delta t_o) + b_o I_b + y_o, \tag{1}$$

where the "$*$" indicates a temporal convolution. The six adjustable parameters are subscripted with "*o*." I_f is a single-exponential decay function, with an amplitude i_o and a decay rate γ_o, that starts at time t_o. When the effects of both stimulated emission and radiation trapping are avoided, as in this work, a single-exponential decay is sufficient to model the LIF.[18] The IRF of the detection electronics is represented by the function *f*, and *g* is a Gaussian function (with a full width at half maximum given by Δt_o) that accounts for the finite laser-excitation dynamics and transit-time spreading due to the extended LIF source. The model also includes the addition of a baseline offset, y_o, and the time-dependent background fluorescence, I_b, scaled by the parameter b_o.

A physically based model for the excitation process affecting the LIF rising edge was not included in Eq. (1). The high-fluence, short-pulse excitation employed here would require a density matrix model[27] with spatial dependence to describe the transient excitation process as a function of position within volume accessed by the LIF collection optics. Such a detailed model was judged unnecessary because the shortest LIF *e*-folding time measured was almost two orders of magnitude greater than the laser pulsewidth. Instead, convolution with the Gaussian function $g(\Delta t_o)$ was used, which produced excellent agreement between the model and data during the leading edge of the decay record with negligible effect on the best-fit values for γ_o.

The measured decay rate includes contributions from quenching of the excited state by each species in the gas mixture and from radiative decay of the excited state (with lifetime τ_{rad}),

$$\gamma_o = \frac{1}{\tau_{\mathrm{rad}}} + \sum_x q_x P_x, \tag{2}$$

where q_x and P_x are the quenching rate coefficient and the partial pressure, respectively, for species *x*.

The gas mixtures typically were composed of high-purity CO, He, and the target quencher species, as well as leak-up gas (LG) resulting from vacuum leaks and outgassing. Equation (2), therefore, can be written explicitly as

$$\gamma_o = \frac{1}{\tau_{\mathrm{rad}}} + q_{\mathrm{CO}} P_{\mathrm{CO}} + q_{\mathrm{He}} P_{\mathrm{He}} + qP + q_{\mathrm{LG}} P_{\mathrm{LG}}, \tag{3}$$

where the unsubscripted symbols correspond to the target quencher species. A corrected decay rate γ_o' is defined as the measured decay rate less the contributions from quenching by CO, He, and LG,

$$\gamma_o' = \gamma_o - (q_{\mathrm{CO}} p_{\mathrm{CO}} + q_{\mathrm{He}} p_{\mathrm{He}} + q_{\mathrm{LG}} p_{\mathrm{LG}}). \tag{4}$$

All terms on the right-hand side of Eq. (4) were experimentally determined; γ_o was determined by fitting the LIF decay, the quenching rate coefficients for CO, He, and LG were all

measured independently in this work, and their partial pressures were recorded during acquisition of the LIF decay.

The corrected decay rate is directly proportional to the partial pressure of the target quenching gas; the constant of proportionality is the quenching rate coefficient, and the zero-pressure intercept is the inverse of the excited-state radiative lifetime,

$$\gamma_o' = \frac{1}{\tau_{\mathrm{rad}}} + qP. \tag{5}$$

Values for τ_{rad} and q were obtained for each quenching pressure sequence using weighted least-squares fits of Eq. (5) to the corrected data.

Thermally averaged quenching cross sections, σ, were calculated from the measured quenching rate coefficients using[21]

$$\sigma = q\sqrt{\frac{\pi\mu k_B T}{8}}, \tag{6}$$

where μ is the reduced mass of the CO/quencher collision pair, k_B is Boltzmann's constant, and T is the absolute temperature.

Finally, a power-law dependence on temperature was used to fit the cross section data for each species,

$$\sigma(T) = \sigma_o\left(\frac{T}{293\,\mathrm{K}}\right)^n. \tag{7}$$

IV. RESULTS

The model described in Eq. (1) was used to fit a total of 1983 measured LIF decays. The 2σ confidence intervals for the best-fit values of γ_o were typically $<1\%$ of γ_o, while scatter in the values of γ_o for decays acquired under the same conditions generally agreed to within 2%. For illustration, a LIF decay and the corresponding fit and fit residual are shown in Fig. 1 [the scaled background, $b_o I_b$ in Eq. (1), has been subtracted for clarity]. An excellent fit is obtained for over two orders of magnitude in signal level, and the model faithfully reproduces the cable reflection at 10 ns. The quenching rate determined from the fit is 175 MHz. This example does not represent the best fit to data that was obtained, but instead demonstrates the quality of the fit to a LIF decay with a lifetime characteristic of the shortest we observed; improved fits were obtained for longer fluorescence lifetimes.

Quenching rates were corrected for the quenching contributions of CO, He, and LG according to Eq. (4). The correction terms due to CO and He were relatively minor ($<0.6\%$ of γ_o) and constant for each pressure sequence, but they were included in the analysis so as not to bias the estimate of τ_{rad} reported here. Fifteen independent measurements of q_{LG} conducted during the course of the experiments were used to estimate the quenching correction due to LG. This correction became increasingly important with increasing temperature. At 1031 K, corrections for LG quenching were $<2.5\%$. Because the LG pressure increases during a quenching pressure sequence, failure to correct for its contribution not only biases the estimate of τ_{rad}, but also causes overestimation of q. In the analysis, the uncertainty of the LG quenching corrections is estimated conservatively to be 50%.

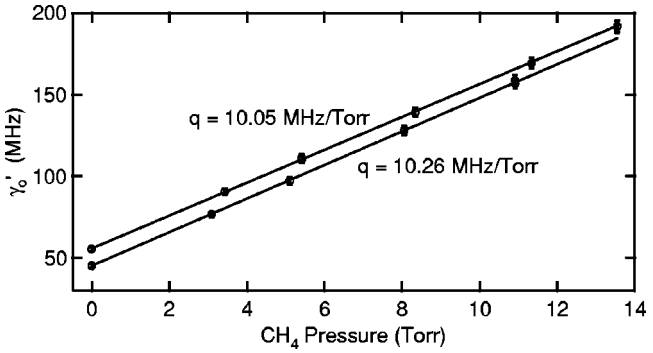

FIG. 2. Example of LIF decay-rate data and corresponding model fits using Eq. (5) for two sequences of CH_4 partial pressure at 1031 K. The top sequence has been offset by 10 MHz for clarity. The best fit values for q are 10.26 and 10.05 MHz/Torr as indicated in the graph.

The corrected quenching rates were plotted against the quenching-gas pressure for 131 pressure sequences. Values for q and τ_{rad} were obtained by fitting Eq. (5) to the corrected data. Typically, the 2σ confidence intervals for the best-fit values of q and τ_{rad} were both $<2\%$. Larger confidence intervals resulted when fitting the quenching rates for the weakest quenchers, He and Ne, because the range of quenching rates observed for these species was limited by the maximum fill pressure of 600 Torr. The weighted average of the best-fit values of τ_{rad} is 22.11 ± 0.04 ns, in agreement with previous reports that properly accounted for radiation trapping (see Ref. 18, and references therein). Values for q obtained for the same quencher and temperature generally agreed to within 2%. For illustration, the data from two partial-pressure sequences of CH_4 at 1031 K are shown in Fig. 2. In this case, the quenching rate constants for the two sequences agree to within 2.1%.

Thermally averaged cross sections were calculated from the measured rate constants using Eq. (6). Table I provides a compilation of the observed cross sections (weighted means of the measurements at each temperature) and the best-fit parameters for the power-law given in Eq. (7). The room-temperature quenching cross sections listed here supercede those reported in an earlier publication by this group.[18] The current and previous measurements of room-temperature cross sections for He, N_2, O_2, CO, H_2O, and CO_2 agree to within the reported experimental uncertainties. The earlier measurements of the room-temperature cross sections for Ar, Kr, Xe, H_2, and CH_4, however, disagreed with those reported here by as much as 17%, and disagreement for Ne was 28%. The values in Table I have been checked for repeatability, and in some cases, several different sources of the quencher gas were used to ensure that a contaminant had not corrupted the data. We attribute the observed discrepancies to the improved analysis scheme used here. Because the earlier analyses applied single-exponential fits to the decays, often over only two time constants, and did not account for the effect of cable reflections, we expect that the previous uncertainties were underestimated.

TABLE I. Measured cross sections for quenching of CO $B\,^1\Sigma^+$ $(v=0)$ and the best-fit parameters for the power-law dependence on temperature given in Eq. (7). Values listed in parentheses represent 2σ uncertainty.

	Quenching cross section (Å^2)				Fit to $\sigma(T)=\sigma_o(T/293)^n$	
Species	293 K	536 K	784 K	1031 K	σ_o(Å^2)	n
He	0.25(0.01)	0.20(0.02)	0.22(0.01)	0.23(0.02)		
Ne	0.42(0.03)	0.42(0.04)	0.47(0.05)	0.51(0.03)		
Ar	32.36(0.40)	28.99(0.56)	26.61(0.42)	24.94(0.42)	32.44(0.43)	−0.20(0.02)
Kr	46.04(0.81)	37.36(0.75)	34.52(0.83)	33.18(0.90)	45.45(0.91)	−0.28(0.03)
Xe	119.3(2.05)	97.01(2.01)	87.79(2.06)	81.94(2.21)	118.6(2.3)	−0.31(0.03)
H_2	9.61(0.21)	13.03(0.18)	15.10(0.22)	16.58(0.31)	9.85(0.20)	0.43(0.02)
N_2	24.46(0.88)	27.31(0.51)	28.40(0.47)	28.81(0.62)	25.10(0.88)	0.12(0.04)
O_2	89.92(1.74)	84.74(1.59)	84.91(1.72)	85.23(6.80)	89.28(2.16)	−0.06(0.04)
CO	36.80(2.09)	36.81(1.69)	37.53(0.95)	37.58(0.57)	36.69(2.38)	0.02(0.06)
H_2O	171.0(3.0)	127.1(2.5)	109.6(2.2)	98.88(2.00)	169.4(3.3)	−0.44(0.02)
CO_2	137.1(2.9)	107.71(2.0)	95.71(2.31)	90.96(2.13)	134.7(3.1)	−0.33(0.03)
CH_4	90.07(1.62)	79.10(1.48)	75.75(1.47)	73.97(1.55)	89.04(1.86)	−0.16(0.03)

The measured cross sections are plotted as a function of temperature for all investigated quenching species in Figs. 3 and 4. Using Eq. (7), fits to the measured cross sections for all species, with the exception of He and Ne, are shown as dotted curves. These interpolating functions reproduce the measured cross sections to within 5%. The curves through the data for He and Ne are only provided for clarity.

V. DISCUSSION

Attaining a full theoretical understanding of quenching of CO $B\,^1\Sigma^+(v=0)$ will be challenging because of the likelihood of contributions from a variety mechanisms, including resonant energy transfer,[21] collision-induced intersystem crossing (CIISC),[28] and charge transfer.[29] In contrast to the widely studied cases of quenching of relatively low-lying electronic states, e.g., NO $A\,^2\Pi$ and OH $A\,^2\Pi$, the CO $B\,^1\Sigma^+$ state has an energy in the vacuum UV ($\sim$86 916 cm^{-1}). The possibility of quenching by resonant energy transfer is enhanced because the higher energy of the CO $B-X$ transition is more likely to lead to overlap with collider absorption bands. Considering such overlaps, energy transfer is a possible channel for H_2O, CO_2, CH_4, O_2, and CO. Again, in contrast with NO and OH, the CO B state is nearly isoenergetic with vibrational levels of CO triplet states.[30] The near degeneracy of the CO $b\,^3\Sigma^+(v=0,1)$ triplet state with $B\,^1\Sigma^+(v=0)$ raises the possibility of CIISC, which would

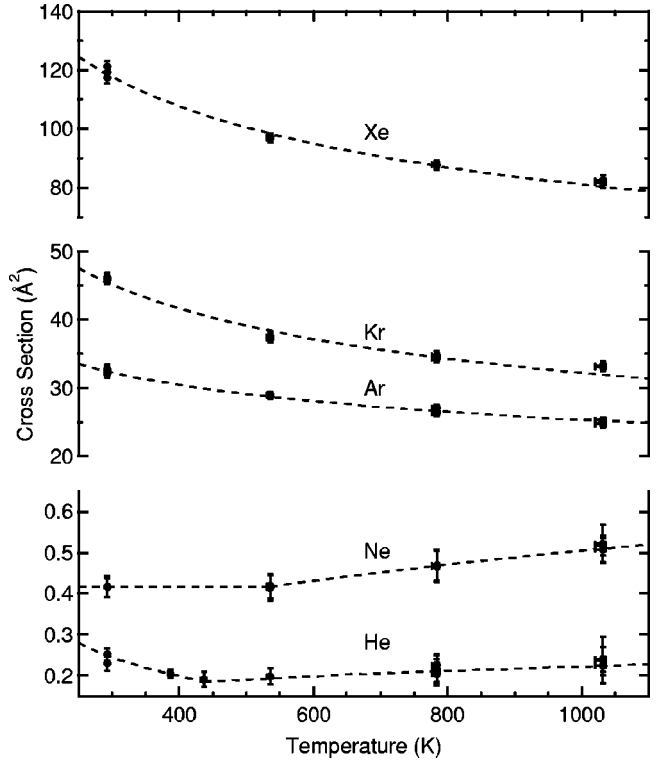

FIG. 3. Thermally averaged cross section for collisional quenching of CO $B\,^1\Sigma^+$ $(v=0)$ by He, Ne, Ar, Kr, and Xe for 293 K$\leqslant T\leqslant$1031 K.

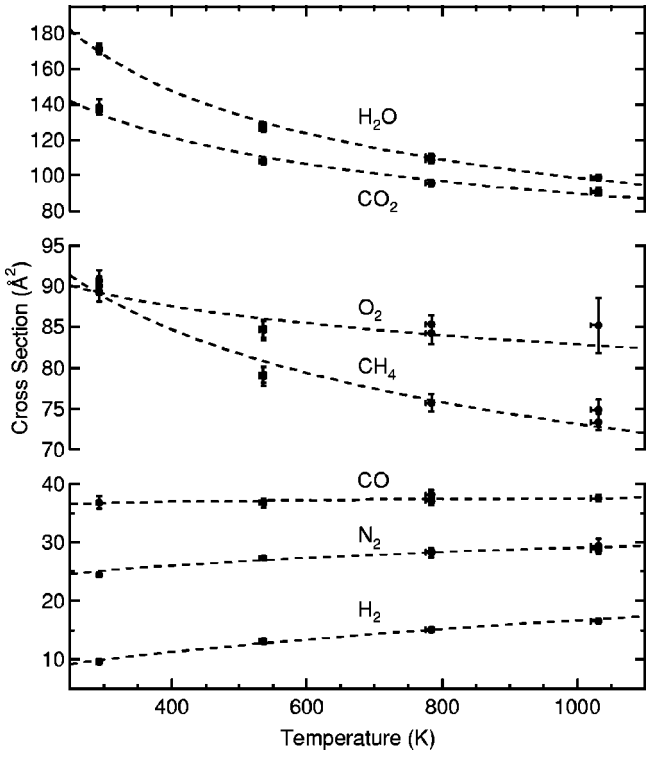

FIG. 4. Thermally averaged cross section for collisional quenching of CO $B\,^1\Sigma^+$ $(v=0)$ by H_2, N_2, O_2, CO, H_2O, CO_2, and CH_4 for 293 K$\leqslant T\leqslant$1031 K.

act to quench fluorescence of the monitored $B-A$ bands. Di Teodoro *et al.*[18] and others[1,8,9,31] have confirmed the presence of CIISC through observation of collision-induced $b\,^3\Sigma^+ \rightarrow a\,^3\Pi$ fluorescence following excitation of the $B\,^1\Sigma^+(v=0)$ state. A third type of quenching mechanism involves transfer of an electron from the emitting molecule to the approaching quencher. Many of the electronic properties of CO $B\,^1\Sigma^+(v=0)$ parallel those of NO $B\,^2\Sigma^+(v=0)$ (both are $3s\sigma$ Rydberg states with roughly similar dipole moments,[32,33] polarizabilities,[34,35] and ionization energies[36]), which has been shown to participate in a charge-transfer (harpoon) quenching mechanism.[29] This mechanism represents a potential quenching channel for species that have stable negative ions, and it is negligibly important for collision partners that have unstable negative ions, i.e., ions subject to rapid autodetachment on a collisional time scale. Therefore the harpoon mechanism may contribute to the observed quenching cross sections for any of the quenchers studied here except for the noble gases, H_2, and CH_4.[29]

The temperature dependences of the measured cross sections vary dramatically for the 12 investigated species. The cross sections of the weakest quenchers (He, Ne, H_2, N_2) increase with temperature, those of the strongest quenchers (H_2O, CO_2, Xe, O_2, CH_4, Kr, Ar) decrease with temperature, and the self-quenching cross section is independent of temperature. The cross section for H_2 has the largest positive temperature dependence, $T^{0.43}$, while H_2O has the largest negative dependence, $T^{-0.44}$.

Quenching by the noble gases is expected to proceed entirely through CIISC (Refs. 18,19) because the harpoon mechanism is inoperative for colliders with unstable negative ions, and the absence of collider transitions at 115 nm precludes resonant energy transfer. Both He and Ne are very weak quenchers, with quenching cross sections that are two orders of magnitude smaller than their hard-sphere cross sections. These findings are in accord with earlier published reports of room-temperature cross sections.[19,20] The strong decrease in the cross section for He between 293 K and 536 K prompted additional measurements at 387 K and 437 K. Between 293 K and 437 K, the cross section for He decreases by 20%, while it slightly increases between 437 K and 1031 K. The Ne cross section also increases slightly in the 536–1031 K range. The other three noble gases considered here (Ar, Kr, Xe) are all effective quenchers of CO. The cross sections for Kr and Ar are on the order of their hard-sphere values, while that for Xe is larger than the hard-sphere value. The power-law exponents characterizing the temperature dependence for the cross sections of Xe, Kr, and Ar are -0.31, -0.28, and -0.20, respectively, indicative of quenching that is governed by attractive forces.[37,38]

Quenching by molecular species H_2O, CO_2, O_2, and CH_4 are all characterized by cross sections that are larger than their hard-sphere values. This result may indicate that a mechanism such as resonant energy transfer contributes to the overall quenching process. The large dipole moment of the CO $B\,^1\Sigma^+$ state (1.95 D) (Ref. 32) should lead to large dipole–dipole interactions with H_2O, and may help to explain a cross section that is 3 times the hard-sphere value at room temperature. The cross section for H_2O decreases strongly with increasing temperature, and is characterized with a power-law exponent of -0.44. The cross sections for CO_2, O_2, and CH_4 also decrease with temperature, presumably because dipole-induced dipole interactions control the quenching.

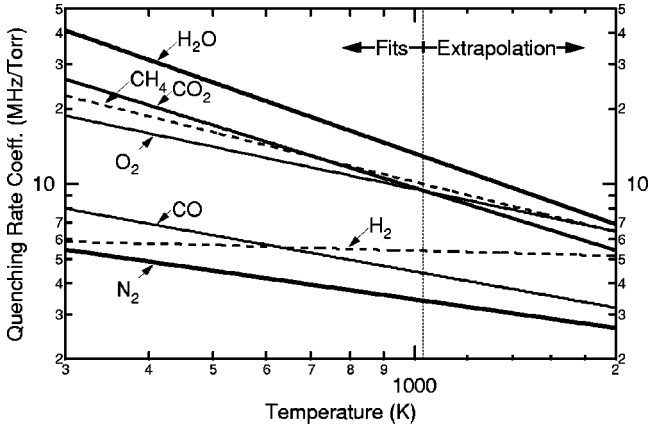

FIG. 5. Quenching rate coefficients for H_2, N_2, O_2, CO, H_2O, CO_2, and CH_4 using Eqs. (6) and (7) and the fit coefficients listed in Table I. The fitting functions have been extrapolated to 2000 K.

The cross section for CO is constant and nearly hard-sphere over the temperature range investigated here. The cross sections for H_2 and N_2 are smaller than their hard-sphere values, but increase with temperature, suggesting that the primary quenching mechanism involves a repulsive interaction potential.

The power-law expressions for the quenching rate coefficients of the important quenching species in a CH_4-air flame are plotted in Fig. 5. The measured quenching rates for CH_4, O_2, CO_2, and H_2O are within 36% of one another at 1031 K. Extrapolations of the fits have been used to predict the quenching rate coefficients for typical flame temperatures. These extrapolations predict that this range narrows with increasing temperature, and the four quenching rate coefficients are within 27% of one another at 2000 K.

The power-law expressions can be used to predict the total quenching rate in an atmospheric-pressure flame. For illustration, we calculate the quenching rate as a function of position in a Tsuji-type[39] counterflow diffusion flame of CH_4 and air. In this system CH_4 flows uniformly from a porous cylindrical burner that is placed in a uniform air stream, and a laminar diffusion flame forms in the forward stagnation region of the cylinder. A detailed flame model (constrained by a measured temperature profile) was used to calculate species concentrations in this flame for a strain rate of 119 s^{-1}.[40] These results were used in the power law expressions for CO quenching rates to predict the total quenching rate in the flame. Figure 6 summarizes the results of these calculations. The total quenching rate, temperature, and CO mole fraction are plotted as functions of distance from the burner. Mixture fraction is shown for reference on the upper axis with the stoichiometric value indicated by f_{ST}. The calculated quenching rate is ~12 GHz in the cold fuel stream and 6.8 GHz in the cold air. The minimum quenching rate is 2.8 GHz and occurs at the temperature peak. Significant quantities of CO exist over the entire temperature range in this

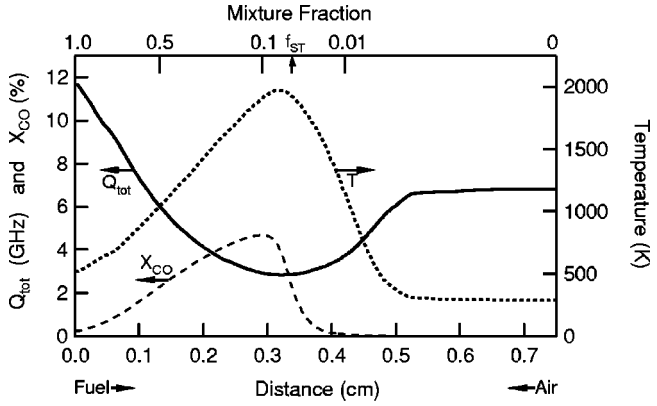

FIG. 6. Calculated quenching rate as a function of distance from the burner in a methane–air counterflow diffusion flame. Mixture fraction is indicated on the upper axis with f_{ST} denoting the stoichiometric value. The total quenching rate is shown by the solid curve, the temperature by the dotted curve, and the CO mole fraction by the dashed curve. The total quenching rate is equal to the sum of the quenching rates computed for H_2, N_2, O_2, CO, H_2O, CO_2, and CH_4.

flame, and CO LIF measurements in this flame are subject to quenching rates that are predicted to vary by a factor of >4. These results demonstrate the wide variability of CO quenching rates in flames and underscore the importance of accurate quenching corrections for quantitative flame measurements of CO using LIF.

VI. CONCLUSIONS

The temperature-dependent quenching cross sections of CO $B\,^1\Sigma^+(v=0)$ in collisions with He, Ne, Ar, Kr, Xe, H_2, N_2, O_2, CO, H_2O, CO_2, and CH_4 were measured using time-resolved, two-photon LIF. Measurements were made at $T=293$ K, 536 K, 784 K, and 1031 K in a temperature-controlled vacuum cell. The species- and temperature-dependent cross sections were fit to a power law, and these fitting functions agreed to within 5% of the measured values for all species except He and Ne. These power-law functions can be used for accurate estimations of the cross sections for $293\ \text{K} \leqslant T \leqslant 1031\ \text{K}$.

Prediction of the total quenching rate in a CH_4–air diffusion flame, using extrapolation of the power-law fits to flame temperatures, demonstrates that quenching corrections for quantitative LIF measurements of CO in flames can vary significantly with temperature and mixture fraction. Such extrapolation must be viewed with caution however, as higher-temperature data are necessary to ensure that the power laws accurately model the cross sections for $T>1000$ K. To this end, we will conduct time-resolved LIF experiments in low-pressure flames.

ACKNOWLEDGMENTS

This work was supported by the Division of Chemical Sciences, Geosciences, and Biosciences, the Office of Basic Energy Sciences, U. S. Department of Energy. In addition, Dr. Dreizler would like to thank Sonderforschungsbereich 568 for support. The authors acknowledge the expert technical assistance of Paul E. Schrader, Sandia National Laboratories.

[1] G. W. Loge, J. J. Tiee, and F. B. Wampler, J. Chem. Phys. **79**, 196 (1983).
[2] J. J. Tiee, M. J. Ferris, G. W. Loge, F. B. Wampler and A. Hartford, *International Congress of Applications of Lasers and Electro-Optics* (Laser Institute of America, Toledo, OH 1982), v. 34, p. 53.
[3] J. Haumann, J. M. Seitzman, and R. K. Hanson, Opt. Lett. **11**, 776 (1986).
[4] J. M. Seitzman, J. Haumann, and R. K. Hanson, Appl. Opt. **26**, 2892 (1987).
[5] D. L. Van Oostendorp, W. T. A. Borghols, and H. B. Levinsky, Combust. Sci. Technol. **79**, 195 (1991).
[6] D. A. Everest, C. R. Shaddix, and K. C. Smyth, 26th Symposium, (International) on Combustion (The Combustion Institute, Pittsburg, P.A. 1996), p. 1161.
[7] N. Georgiev and M. Aldén, Appl. Spectrosc. **51**, 1229 (1997).
[8] M. Aldén, S. Wallin, and W. Wendt, Appl. Phys. B: Photophys. Laser Chem. **33**, 205 (1984).
[9] U. Westblom, S. Agrup, M. Aldén, H. M. Hertz, and J. E. M. Goldsmith, Appl. Phys. B: Photophys. Laser Chem. **50**, 487 (1990).
[10] S. Agrup and M. Aldén, Chem. Phys. Lett. **189**, 211 (1992).
[11] S. Agrup and M. Aldén, Appl. Spectrosc. **48**, 1118 (1994).
[12] A. V. Mokhov, H. B. Levinsky, C. E. van der Meij, and R. A. A. M. Jacobs, Appl. Opt. **34**, 7074 (1995).
[13] A. P. Nefedov, V. A. Sinel'shchikov, A. D. Usachev, and A. V. Zobnin, Appl. Opt. **37**, 7729 (1998).
[14] A. V. Zobnin, A. P. Nefedov, V. A. Sinel'shchikov, and A. D. Usachev, Opt. Spectrosc. **87**, 23 (1999).
[15] G. J. Fiechtner, C. D. Carter, and R. S. Barlow, in Proceedings of the 33rd National Heat Transfer Conference, 15–17 August, Albuquerque, New Mexico, 1999, p. 1.
[16] L. Gasnot, P. Desgroux, J. F. Pauwels, and L. R. Sochet, Combust. Flame **117**, 291 (1999).
[17] A. V. Mokhov, A. P. N. Nefedov, B. V. Rogou, V. A. Sinel'shehinov, and H. B. Levinsky, Combust. Flame **119**, 161 (1999).
[18] F. Di Teodoro, J. E. Rehm, R. L. Farrow, and P. H. Paul, J. Chem. Phys. **113**, 3046 (2000).
[19] F. J. Comes and E. H. Fink, Z. Naturforsch. A **28A**, 717 (1973).
[20] S. S. Dimov and C. R. Vidal, Chem. Phys. Lett. **221**, 307 (1994).
[21] J. T. Yardley, *Introduction to Molecular Energy Transfer* (Academic, New York, 1980).
[22] X. Ma and R. Lai, Phys. Rev. A **49**, 787 (1994).
[23] Z. Bor, Opt. Commun. **29**, 103 (1979).
[24] P. P. Yaney, D. A. V. Kliner, P. E. Schrader, and R. L. Farrow, Rev. Sci. Instrum. **71**, 1296 (2000).
[25] A. E. Lutz, R. J. Kee, and J. A. Miller, SAND87–8248, Sandia National Laboratories, Livermore, CA 94551, 1997.
[26] Program No. 307, Quantum Chemistry Program Exchange, Indiana University, Bloomington, IN 47401.
[27] T. B. Settersten and M. A. Linne, J. Opt. Soc. Am. B **19**, 954 (2002).
[28] K. F. Freed, Adv. Chem. Phys. **47**, 291 (1981).
[29] P. H. Paul, J. A. Gray, J. L. Durant, and J. W. Thoman, Appl. Phys. B: Photophys. Laser Chem. **57**, 249 (1993).
[30] G. Herzberg, *Molecular Spectra and Molecular Structure. I. Spectra of Diatomic Molecules* (Kreiger, Malabar, 1989), pp. 452–453.
[31] L. F. DiMauro and T. A. Miller, Chem. Phys. Lett. **138**, 175 (1987).
[32] M. Drabbels, W. L. Meerts, and J. J. ter Meulen, J. Chem. Phys. **99**, 2352 (1993).
[33] J. A. Gray, R. L. Farrow, J. L. Durant, and L. R. Thorne, J. Chem. Phys. **99**, 4327 (1993).
[34] M. D. Di Rosa and R. L. Farrow, J. Quant. Spectrosc. Radiat. Transf. **68**, 363 (2001).
[35] M. D. Di Rosa and R. K. Hanson, J. Mol. Spectrosc. **164**, 97 (1994).
[36] A. A. Radzig and S. M. Smirnov, *Reference Data on Atom, Molecules, and Ions* (Springer, New York, 1985).
[37] D. L. Holtermann, E. K. C. Lee, and R. Nanes, J. Chem. Phys. **77**, 5327 (1982).
[38] M. R. Furlanetto, J. W. Thoman, J. A. Gray, P. H. Paul and J. L. Durant, J. Chem. Phys. **101**, 10452 (1994).
[39] H. Tsuji, Prog. Energy Combust. Sci. **8**, 93 (1982).
[40] J. Driscoll, V. Sick, R. L. Farrow, and P. E. Schrader, *29th Symposium (International) on Combustion* (The Combustion Institute, Pittsburgh, P.A. 2002), in press.